CCFE-PR(15)46

Hyun-Tae Kim, M. Romanelli, I. Voitsekhovitch, T. Koskela, J. Conboy,
C. Giroud, G. Maddison, E. Joffrin, and JET contributors

Comparative Analysis of Core Heat Transport of JET High Density H-mode Plasmas in Carbon Wall and ITER-Like Wall

Comparative Analysis of Core Heat Transport of JET High Density H-mode Plasmas in Carbon Wall and ITER-Like Wall

Hyun-Tae Kim[1,2], M. Romanelli[1], I. Voitsekhovitch[1], T. Koskela[3], J. Conboy[1], C. Giroud[1], G. Maddison[1], E. Joffrin[4], and JET contributors[*]

[1]CCFE, Culham Science Centre, Abingdon, Oxon, OX14 3DB, UK
[2]Department of Physics, Imperial College London, SW7 2AZ, London, UK
[3]Aalto University, Association EURATOM-Tekes, P.O.Box 14100, FIN-00076 Aalto, Finland
[4]CEA, IRFM, F-13108 Saint-Paul-lez-Durance, France

Comparative Analysis of Core Heat Transport of JET High Density H-mode Plasmas in Carbon Wall and ITER-Like Wall

Hyun-Tae Kim[1,2], M. Romanelli[1], I. Voitsekhovitch[1], T. Koskela[3], J. Conboy[1], C. Giroud[1], G. Maddison[1], E. Joffrin[4], and JET contributors*

EUROfusion Consortium, JET, Culham Science Centre, Abingdon, OX14 3DB, UK

[1] *CCFE, Culham Science Centre, Abingdon, Oxon, OX14 3DB, UK*

[2] *Department of Physics, Imperial College London, SW7 2AZ, London, UK*

[3] *Aalto University, Association EURATOM-Tekes, P.O.Box 14100, FIN-00076 Aalto, Finland*

[4] *CEA, IRFM, F-13108 Saint-Paul-lez-Durance, France*

* See the Appendix of F. Romanelli et al., Proceedings of the 25th IAEA Fusion Energy Conference 2014, Saint Petersburg, Russia

A consistent deterioration of global confinement in H-mode experiments has been observed in JET [1] following the replacement of all carbon Plasma Facing Components (PFCs) with an all metal ('ITER-like') wall (ILW). This has been correlated to the observed degradation of the pedestal confinement, as lower electron temperature (T_e) values are routinely measured at the top of the edge barrier region. A comparative investigation of core heat transport in JET-ILW and JET-CW (Carbon Wall) discharges has been performed, to assess whether core confinement has also been affected by the wall change.

The results presented here have been obtained by analysing a set of discharges consisting of high density JET-ILW H-mode plasmas and comparing them against their counterpart discharges in JET-CW having similar global operational parameters. The set contains 10 baseline (β_N =1.5~2) discharge-pairs with 2.7 T toroidal magnetic field, 2.5 MA plasma current, and 14 to 17MW of Neutral Beam Injection (NBI) heating.

Based on a T_e profile analysis using High Resolution Thomson Scattering (HRTS) data, the T_e profile peaking (i.e. core T_e (ρ=0.3) / edge T_e (ρ =0.7)) is found to be similar, and weakly dependent on edge T_e, for both JET-ILW and JET-CW discharges. When ILW discharges are seeded with N_2, core and edge T_e both increase to maintain a similar peaking factor.

The change in core confinement is addressed with interpretative TRANSP simulations. It is found that JET-ILW H-mode plasmas have higher NBI power deposition to electrons and lower NBI power deposition to ions as compared to the JET-CW counterparts. This is an effect of the lower electron temperature at the top of the pedestal. As a result, the core electron energy confinement time is reduced in JET-ILW discharges, but the core ion energy confinement time is not decreased. Overall, the core energy confinement is found to be the same in the JET-ILW discharges compared to the JET-CW counterparts.

1 INTRODUCTION

Carbon Plasma Facing Components (PFCs) have been recently replaced in JET with an all metal Beryllium first wall and Tungsten divertor, which comprise the ILW (ITER-Like Wall) [2]. It is well known that the interaction between plasma and the surrounding wall can influence plasma energy confinement significantly as a result of the sputtering of different impurities and modified wall recycling [1]. In addition, the operational techniques required for the ILW (e.g. higher gas fuelling, to avoid W accumulation in the core) differ from those required for CW (Carbon Wall) operation. After the wall change, the global energy confinement in JET-ILW was routinely found to be degraded, when compared to similar plasmas in the CW configuration. A similar confinement loss was also reported in ASDEX-Upgrade after the installation of the full tungsten wall [3] . In both devices, the core temperatures are found to be lower as are the temperatures at the top of the pedestal [3] [4]. These observations have an impact on the extrapolation to ITER plasma performances as a full metal wall (Be first wall and Tungsten divertor) is planned in ITER. One current research topics at JET-ILW is therefore the investigation of the cause for this deterioration [1] [4]. It is well known that the core temperature depends on the temperature at the plasma edge. Since the edge temperature is lower in the ILW configuration, it is not obvious whether the decrease in core temperature is only due to the degradation of the edge confinement or if the core confinement itself has also been degraded.

A heat transport analysis of 10 pairs of counterpart discharges (10 CW discharges and 10 corresponding ILW discharges), has been carried out to address this question. Counterpart discharges have been carefully selected to match the time-averaged value of the controllable global plasma parameters -

- 2.5MA of total plasma current I_p,
- 2.7T of toroidal magnetic field B_t,
- 14 - 17MW of applied NBI power $P_{NBI,}$
- 7.1-10.2 x $10^{19}m^{-3}$ volume-averaged electron density $< n_e >$
- safety factor q_{95},
- triangularity δ

- as closely as possible within a reference time window, from t_{ref} - 0.5 s to t_{ref} +0.5 s. The reference time t_{ref} is selected during the stationary flat-top phase of the discharge (see Figure 1(a), (b), (c), (d), and (e)). Core MHD activity in the selected discharges is not significant enough to affect core transport within the analysed interval. Figure 1 (f)(g) shows that the core T_e and n_e are in steady state with only small-amplitude fluctuations around the average value. The counterpart discharge selection is designed to remove the influence of the global plasma parameters, and allow an investigation of the effects of the different walls on transport processes. It is observed that Z_{eff} in CW shots is much higher than Z_{eff} in the ILW counterparts i.e. Z_{eff} = 1.7~2.4 for CW and Z_{eff} = 1.1~1.3 for ILW. This indicates that the plasma compositions in CW and ILW are different. For CW discharges, Z_{eff} is subject to significant variation even without any impurity seeding. This can be attributed not only to the wall material, but also to the impurity retention from the previous impurity-seeded discharges. On the other hand, the Z_{eff} variation in the ILW discharges is much less significant allowing a higher degree of reproducibility, although small variation can still exist when the discharges are following after impurity-seeded discharges on the same day. It should be noted that the highest Z_{eff} in unseeded ILW discharges is still smaller than the lowest Z_{eff} in CW, but with N_2 seeding in ILW discharges the Z_{eff} increases up to a comparable value in CW.

The analysis reported in this paper is focused on low beta baseline H-mode plasmas. Figure 1 shows a typical example of the counterpart discharges selected *amongst low beta baseline (β_N =1.5~2) H-mode plasmas, which have high plasma density (*$7\times10^{19}m^{-3} < \bar{n}_e \le n_{GW} \approx 9\times10^{19}m^{-3}$*).* At these level of collisionality, the electron and ion temperature profiles tend to be very similar because of the high equilibration power i.e. $T_e \approx T_i$. High beta hybrid ($\beta_N \approx 3$) plasmas [5] have been analysed in Challis et al [6], where it is reported that the power degradation of thermal energy confinement with heating power is weaker in JET-ILW discharges. The main parameters of the discharges analysed are given in Table 1. In order to minimise the effect of measurement errors, time averaged values are used in this study.

In section 2 we report the comparison of the High Resolution Thomson Scattering T_e profiles between JET-ILW and JET-CW discharges. In section 3, the interpretive analysis of

core confinement, using the TRANSP transport analysis code [7] [8] is presented. Discussions and Conclusions are given in sections 4 and 5, respectively.

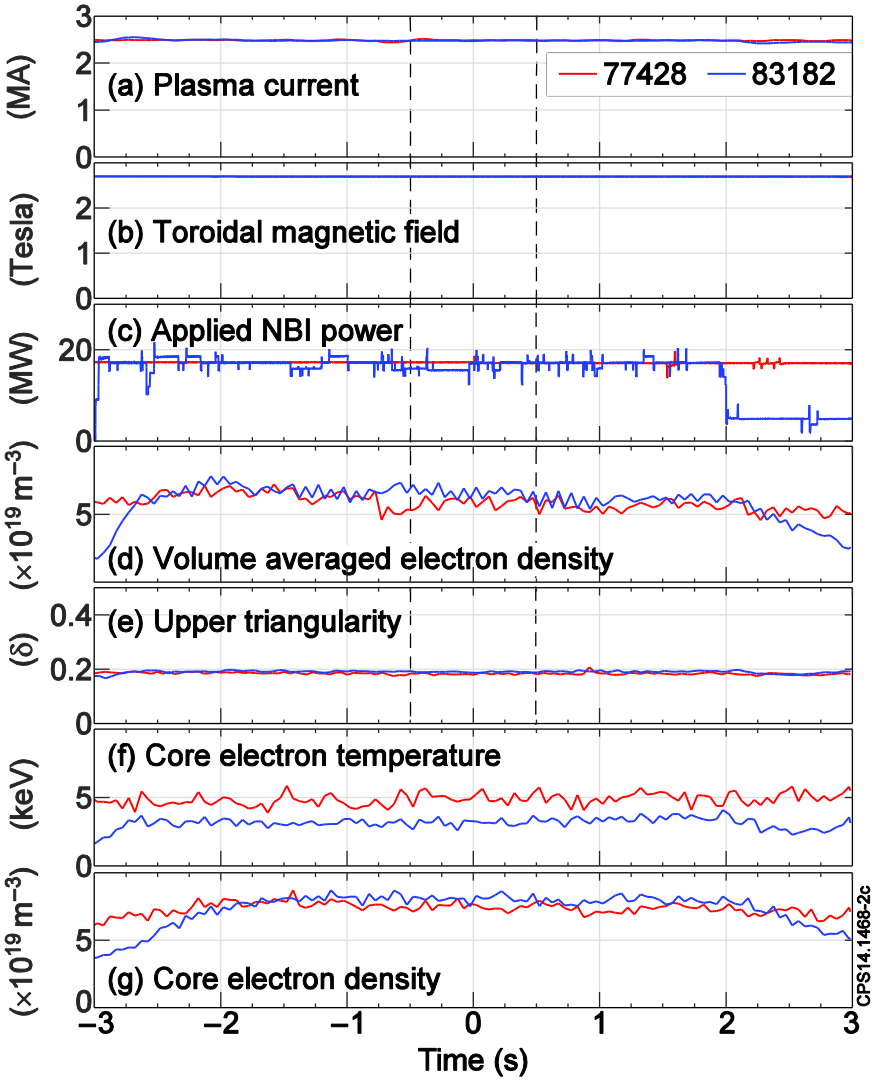

Figure 1. A typical example of counterpart H-mode plasmas in CW (#77428, Red) and ILW (#83182, Blue). The counterpart discharges having similar controllable global parameters – (a) plasma current I_p, (b) Toroidal magnetic field B_t, (c) Applied NBI power P_{NBI}, (d) Volume averaged electron density $<n_e>$, q_{95}, and (e)Upper triangularity δ - around the reference time t_{ref} (indicated with 0). The vertical dashed lines show the averaged time interval for selection of counterpart discharges. (f) Core T_e and (g) n_e at R=3.2m are measured by HRTS.

	Shot	t_ref	Bt [T]	Ip [MA]	Applied P_NBI [MW]	$<\varepsilon_b/T_e>$ ρ<0.5	Applied P_ICH [MW]	<Te> [keV] (ρ<0.5)	<ne> [1e20 m-3] (ρ<0.5)	<Zeff>	upper δ at ρ=1
CW	79453	20	2.7	2.5	14	13	1	3.6	0.92	2.09	0.45
ILW(N2)	82819	15	2.7	2.48	16	15	0	3.0	0.92	1.72	0.40
CW	79435	20	2.7	2.5	14	16	0	3.0	1.02	1.69	0.44
ILW(N2)	82811	15	2.7	2.48	16.4	17	0	2.6	0.98	1.79	0.39
CW	77428	15	2.7	2.5	17	12	0	4.2	0.71	1.58	0.18
ILW(N2)	83182	15	2.7	2.48	16	17	0	2.7	0.79	1.50	0.19
CW	79747	16	2.7	2.5	15	13	0	3.5	0.72	1.80	0.18
ILW	83175	15	2.7	2.5	14.8	18	0	2.4	0.83	1.11	0.19
CW	79441	20	2.7	2.5	14	14	1	3.2	0.90	1.65	0.44
ILW	82751	15	2.7	2.48	16	19	0	2.2	0.81	1.26	0.38
CW	77424	15	2.7	2.5	15	12	0	4.3	0.71	2.38	0.18
ILW	83177	15	2.7	2.47	16.7	19	0	2.3	0.82	1.23	0.18
CW	74312	20	2.7	2.5	14	15	1	3.8	0.86	1.59	0.43
ILW	85406	12	2.7	2.5	16.4	19	0	2.3	0.80	1.04	0.37
CW	74313	20	2.7	2.5	15	18	1	2.9	0.89	1.65	0.41
ILW	85407	12	2.7	2.5	15.6	20	0	2.2	0.84	1.03	0.37
CW	76666	20	2.7	2.5	14.9	14	1.2	3.6	0.91	1.93	0.44
ILW*	82549	15	2.7	2.5	15	19	2	2.3	0.86	1.27	0.38
CW*	76677	20	2.7	2.5	13.9	14	1.7	3.7	0.96	1.95	0.44
ILW*	82558	15	2.6	2.6	14.9	19	1.4	2.4	0.79	1.25	0.38

*Table 1 Plasma parameters of counterpart discharges in Carbon Wall and in ITER-Like Wall. (N2) shows N_2 seeded discharges. * indicates (unseeded) discharges after seeded discharges on the same day.*

2 ELECTRON TEMPERATURE PROFILE ANALYSIS

Electron temperature (T_e) profiles measured by the High Resolution Thomson Scattering (HRTS) system are used in the present study [9]. Figure 2 shows that the T_e profiles are fitted using a constrained optimisation method based on tomographic techniques (this method optimises the smoothness function while the calculated profile is constrained by measurements [10]), and then remapped to the flux coordinate computed by EFIT [11]. Figure 3 shows T_e profiles at each reference time t_{ref} (at which each pair of counterpart shots has similar global parameters). The profiles have a constant local temperature gradient in the radial region between ρ=0.3~0.7, which enables them to be compared using the temperature ratio between the two fixed end points. ρ is the square root of normalized toroidal flux,

$\sqrt{\Phi_N}$. In this paper, the temperature ratio (i.e. T_e peaking) is defined as $T_e(\rho=0.3)/T_e(\rho=0.7)$. Figure 3 shows that for the same controllable global parameters (i.e. applied NBI power, I_p, B_t, $<n_e>$, q, and δ), JET-CW discharges have steeper T_e profiles than the JET-ILW counterparts without any exception. Figure 4 shows the corresponding pressure profiles. As $<n_e>$ is one of the matching criteria for the selection of counterpart discharges, the steeper pressure profiles in JET-CW discharges result from steeper T_e profiles.

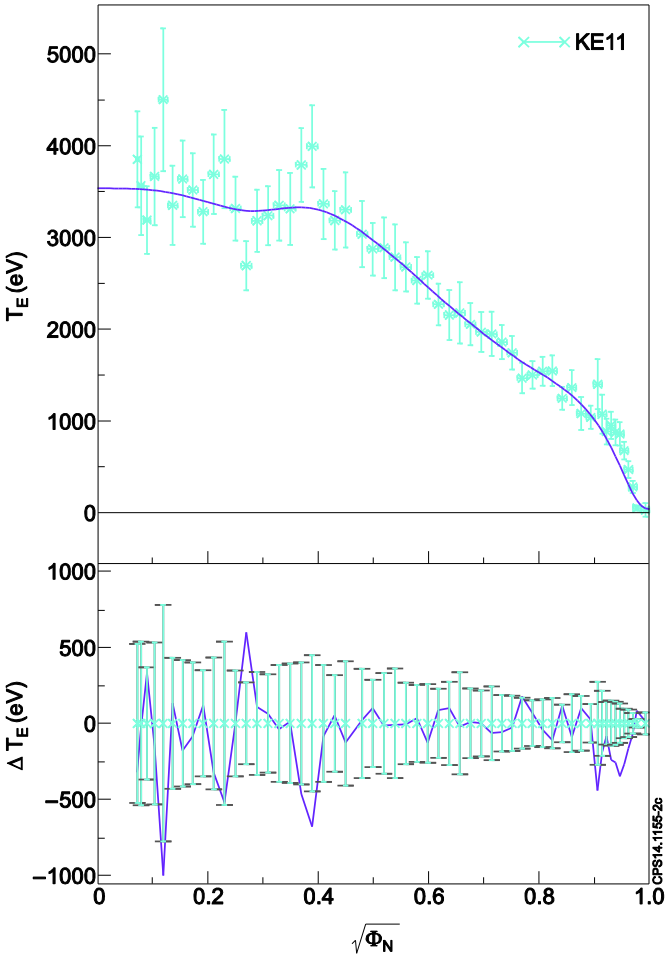

Figure 2 Remapped HRTS T_e profile (#82819, 55seconds). ΔT_e shows the deviation of the fitting lines from measured data points.

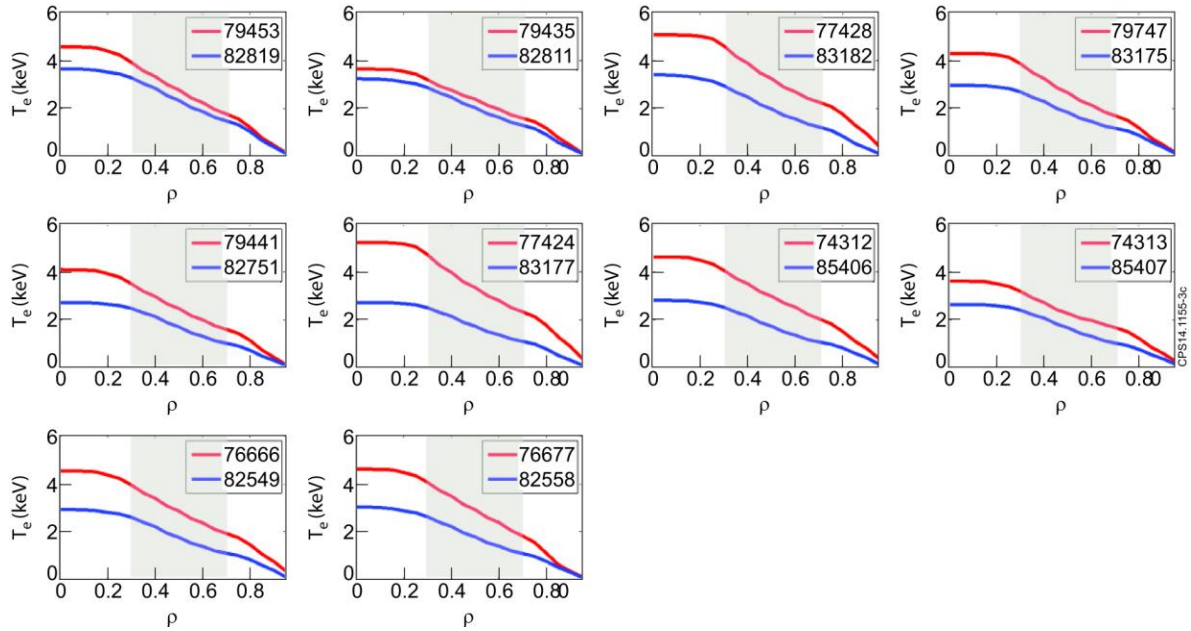

Figure 3 Electron temperature profiles of counterpart discharges in CW (red) and ILW (blue) measured by HRTS (High Resolution Thomson Scattering) and mapped on TRANSP radial coordinate (fitting applied). In the analysed region (i.e. ρ=0.3~0.7), T_e profiles show a linear increase, justifying the profile analysis based on T_e peaking (i.e. $T_e(\rho=0.3)/T_e(\rho=0.7)$).

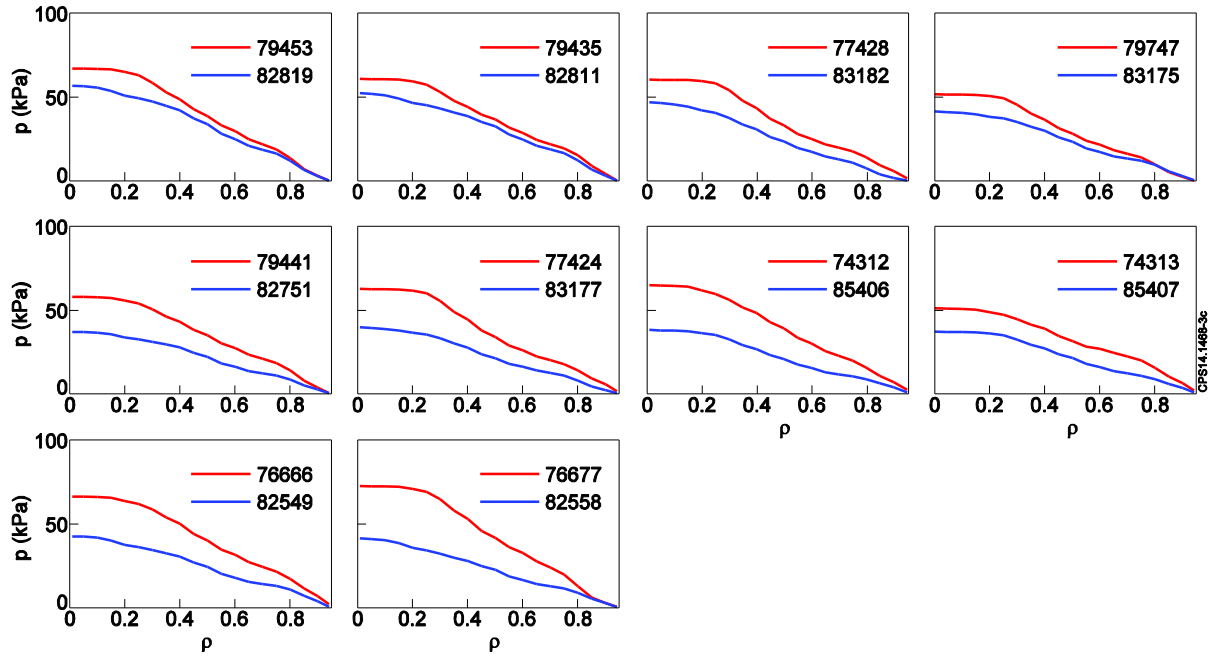

Figure 4 plasma pressure (=n_e x T_e) profiles of counterpart discharges in CW (red) and ILW (blue). n_e and T_e used for calculation are measured by HRTS. The profiles are mapped as in Figure 3.

Figure 5 shows the variation of core temperature with edge temperature. The error bars σ_i are calculated considering statistical and systematic errors of the HRTS measurement, i.e. $\sigma_i^2 = \sigma_{SEM}^2 + \sigma_{SYS}^2 = \sigma_{sta}^2 / N + (0.05 \times T_e^{core})^2$. σ_{SEM} is the standard error of the mean, which is calculated as $\sigma_{SEM}^2 = \sigma_{sta}^2 / N$ where σ_{sta} is the standard deviation. Here, N=10 as T_e data used is an averaged value over 10 data points for the reference time window. The systematic error σ_{SYS} is calculated as $\sigma_{SYS}^2 = (0.05 \times T_e^{core})^2$, assuming a 5% uncertainty in HRTS T_e measurement comparisons between the ILW and C walls. The fit error in Figure 2 is not included to calculate the error bar in Figure 5 as they are small enough to be ignored for the analysed radial interval. In addition, a few data points deviated from the fit are removed in the time-averaged data.

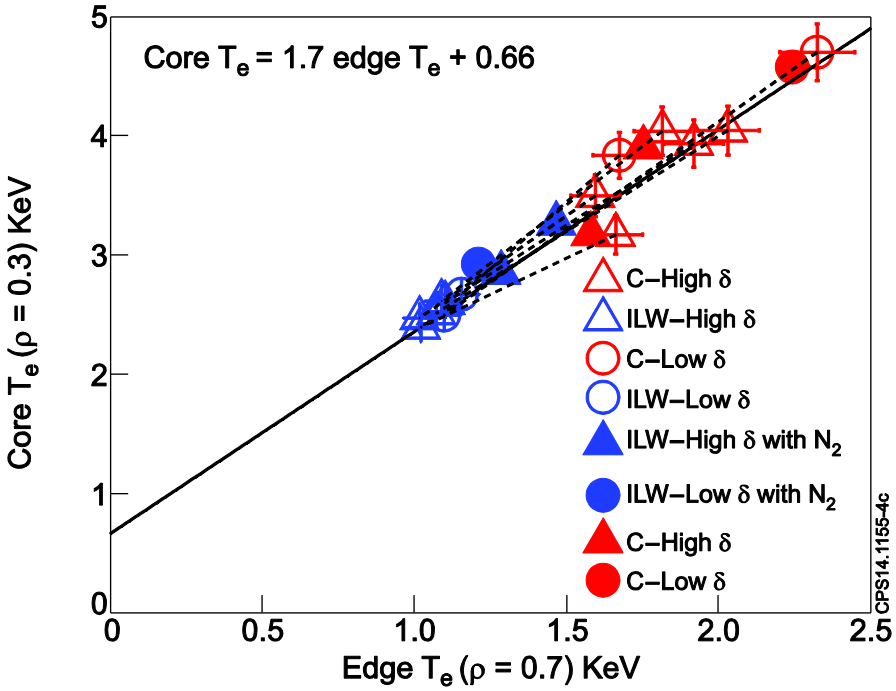

Figure 5 Core T_e (ρ=0.3) vs Edge T_e (ρ=0.7). The blue and red symbols indicate ILW and CW plasmas respectively. Dashed lines indicate the change from CW to the counterpart ILW discharge for N_2 seeded plasmas. Blue filled symbols are N_2 seeded ILW plasmas, and red filled symbols are their counterparts in CW. Blank symbols are without impurity seeding. The triangles and circles indicate high and low δ, respectively. The black solid line is a linear fit to the unseeded ILW+CW plasmas, and shows that the N_2 seeded plasmas are positioned between the unseeded ILW and CW discharges.

The dashed lines in Figure 5 indicate the change from each CW to its counterpart ILW discharge. As discussed in the introduction, the core T_e is found to be lower in ILW, and this is accompanied by the decrease in edge T_e. An important point to note is that both ILW and CW data are well represented by the same linear fit, showing that the T_e peaking is not significantly modified by the change of PFCs.

Recently it has been observed in JET-ILW that nitrogen seeding can help to recover the edge T_e, and the core T_e in turn, although the full recovery of edge T_e to the previous value has not yet been achieved [12]. A similar result was also reported in N_2 seeded plasmas in ASDEX-Upgrade [3]. The seeding of N_2 in ILW discharges (blue filled symbols) has the effect of moving the profiles towards the CW counterparts, along the same trend line – suggesting that the decrease in core T_e for the ILW discharges is due only to the decrease in edge T_e, and not to any degradation in the T_e peaking.

3 TRANSPORT ANALYSIS

3.1 Input and assumptions for TRANSP analysis

Core transport has been analysed by using the TRANSP code [7] [8]. For these simulations, electron density and temperature profiles are taken from HRTS (High Resolution Thomson Scattering) measurements. Ion temperature (T_i) data is not available in most of the analysed discharges. T_i is assumed to be equal to T_e based on the high densities of the selected discharges ($< n_e > > 7\text{x}10^{19}\text{m}^{-3}$). Figure 6 shows a sample case in the database, for which the ion temperature measurement by Charge Exchange Radiation was available. The comparison show that $T_i = T_e$ is a reasonable assumption for the analysed discharges. The dominant impurity is determined by the PFC material i.e. Carbon for JET-CW, and Beryllium for JET-ILW. The impurity density profile is calculated to be proportional to the electron density assuming a uniform Z_{eff} over the whole radius, where Z_{eff} is determined from visible Bremsstrahlung [13]. The bulk radiation input is given by Bolometry measurement [14]. NBI and RF heating are calculated by NUBEAM [7] and TORIC [15], respectively. The q profile is taken from the equilibrium reconstructed by EFIT [11], constrained by the magnetic probe measurements.

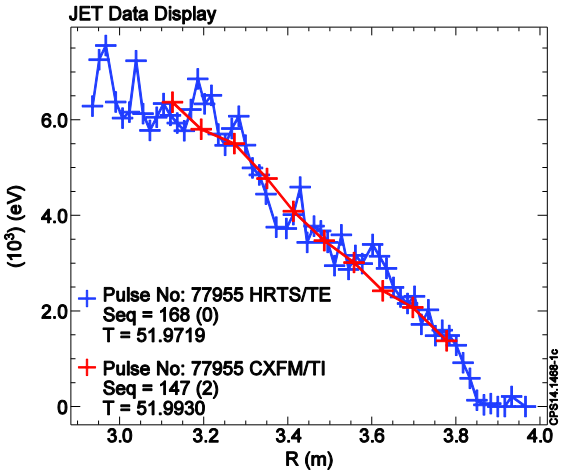

Figure 6 Profiles of T_i measured by Charge Exchange Radiaiton (CXFM/TI) and T_e measured by HRTS (HRTS/TE) at 52 seconds in #77955, which is one of the analysed discharges.

3.2 Comparison of transport properties

Electron and ion heat fluxes q_e , q_i, and heat conductivities χ_e , χ_i are key transport properties to quantify core confinement. However, these transport properties are not measurable directly from experiments. In this paper, the transport properties are calculated by interpretative TRANSP simulations, using the measured input data – {T_e, n_e, P_{rad}, Z_{eff}, I_p, V_{loop}, B_t, applied P_{NBI}, applied P_{RF}, Gas puffing rate, Last Closed Flux Surface (LCFS) } [16]. It should be noted that heat fluxes and conductivities are calculated by solving the energy balance equation. The energy balance equation of electrons is [17]

$$\frac{3}{2}\frac{\partial(n_e T_e)}{\partial t} + \nabla\cdot\Big(\underbrace{\vec{q}_e}_{\text{conductive heat flux}} + \underbrace{\frac{5}{2}\vec{\Gamma}_e T_e}_{\text{convective heat flux}}\Big) = P_e^{\text{source}} \qquad (1)$$

where the electron conductive heat flux is defined as $\vec{q}_e \equiv -\chi_e n_e \nabla T_e$, and ohmic heating, auxiliary heating such as NBI and RF, equilibration power loss, and atomic reaction related power losses are included in the source term ($P_e^{\text{source}} = P_{oh}^e + P_{NBI}^e + P_{RF}^e - P_{equi}^e - P_{iz}^e - P_{rad}^e - P_{rec}^e$). $n_e(\rho,t)$ and $T_e(\rho,t)$ are given by measured input profiles, and the source terms are either functions of $n_e(\rho,t)$ and $T_e(\rho,t)$ or directly given by measurements e.g. P_{rad}. The particle flux $\vec{\Gamma}_e$ appearing in the convective heat flux is calculated by solving the continuity equation, the balance between the particle sources and losses computed in TRANSP using the measured

data. Rearranging equation (1) and integrating over the volume enclosed by the flux coordinate ρ allows one to obtain the radial electron heat flux $\overrightarrow{q_e} \cdot \hat{\mathrm{r}}$ and in turn $\chi_e (= -(\overrightarrow{q_e} \cdot \mathrm{r}) / (n_e \nabla T_e \cdot \hat{\mathrm{r}}))$, which is consistent with the input profiles of T_e and n_e.

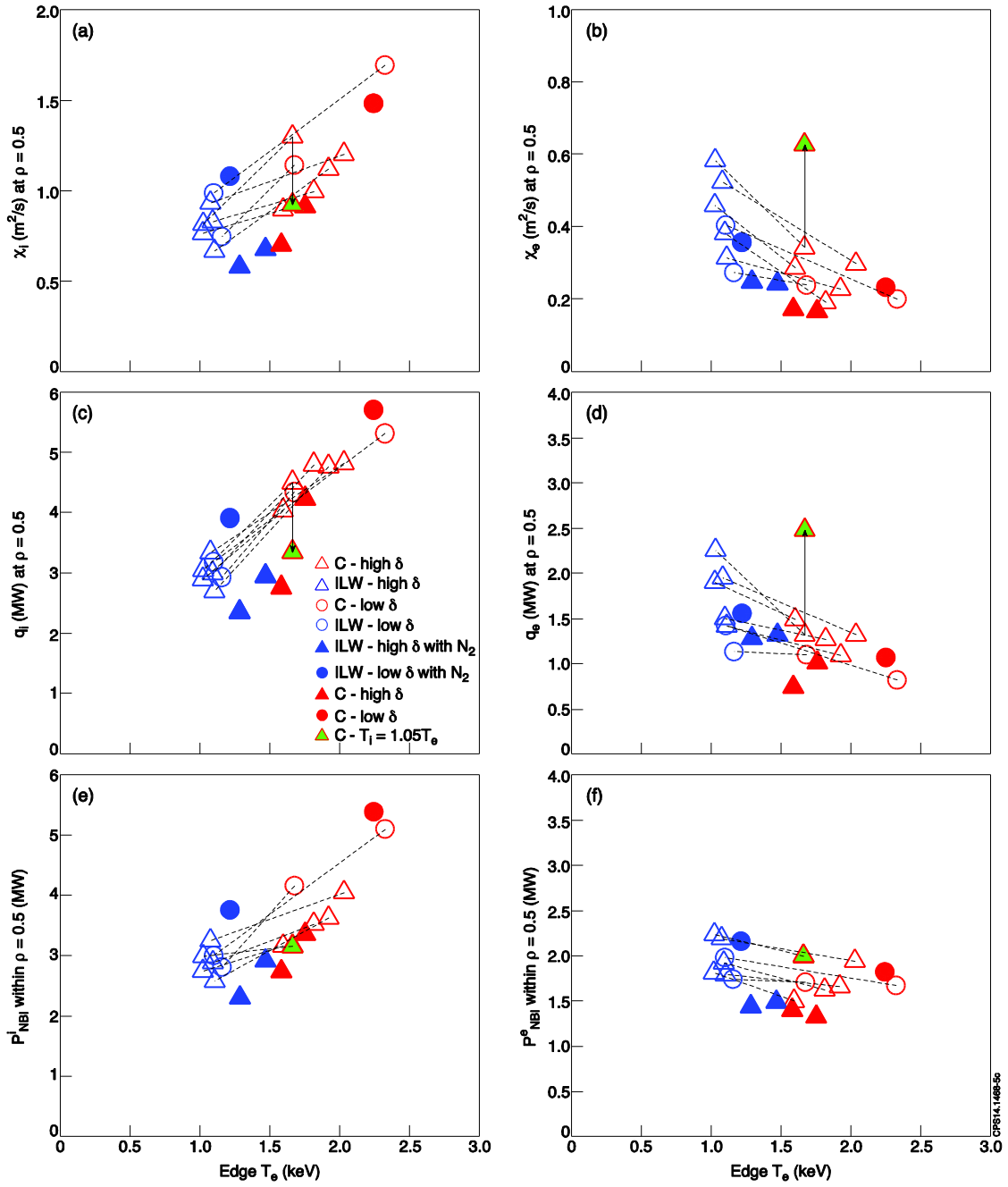

Figure 7 (a)(b) Heat conductivity of ion χ_i and electron χ_e at $\rho = 0.5$ vs edge T_e (c)(d) Total heat flux of ion q_i and electron q_e at $\rho = 0.5$ (e)(f) NBI power deposition to ion P^i_{NBI} and electron P^e_{NBI} within the volume $\rho < 0.5$. For all figures x axis is edge T_e at $\rho = 0.7$. Each

dashed line indicates the counterpart data to show the change of the data from JET-CW to JET-ILW. The green filled triangles indicate the TRANSP results with T_i=1.05T_e.Otherwise, the notation of colour and symbols are same as described in Figure 5.

Figures 7(a) and (b) show the TRANSP calculated conductivities χ_e and χ_i at ρ=0.5. As indicated by the dashed lines, there is a consistent change of conductivities from JET-CW to JET-ILW i.e. an increase in χ_e and decrease in χ_i . Figures 7(c) and (d) show that the total radial heat fluxes for electrons (q_e) and ions (q_i) at ρ=0.5 have similar trends. Although $n_e\nabla T_e$ is higher in CW data ($<n_e>$ is one of the matching criteria, but ∇T_e is higher in CW), this does not significantly affect the variation of χ_e and χ_i between CW and ILW. The observed trend of q_e and q_i can be correlated to the change in NBI power deposition. TRANSP calculates the deposited power with NUBEAM, a NBI module using a Monte Carlo method, which takes into account effects such as shine-though power, Charge Exchange losses, and orbital drift losses [7].

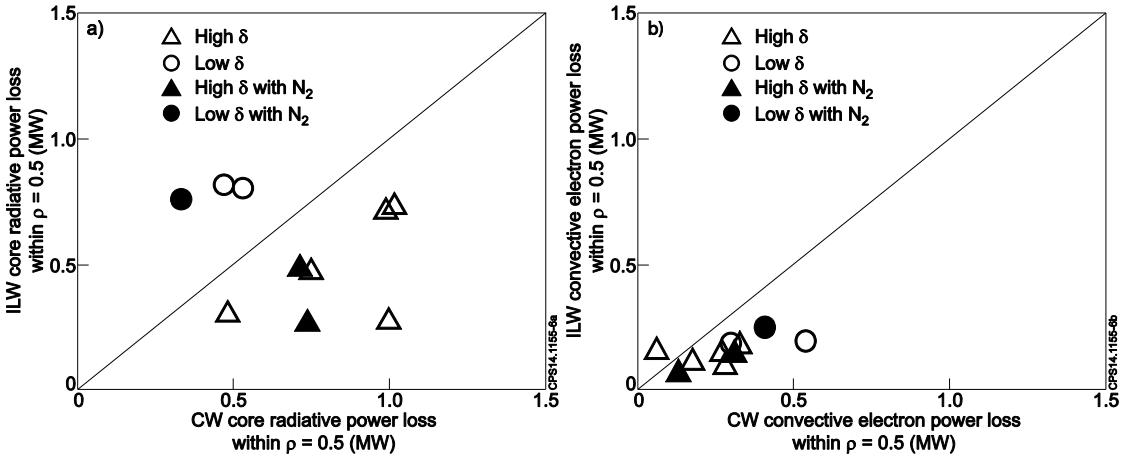

Figure 8 (a) Core radiation comparison within the volume ρ < 0.5 between CW (x axis) and ILW (y axis). (b) Convective electron power loss within the volume ρ < 0.5 between CW (x axis) and ILW (y axis). Triangle and circles are high and low δ , and the filled and blank symbols indicate N_2 seeded and unseeded plasmas, respectively.

Figure 7(e) and (f) show the TRANSP calculated NBI power deposition to electrons and ions, integrated over the volume ρ <0.5. The NBI heating power to the ions P_{NBI}^{i} not only shows the qualitative trend of change seen for q_i but also the same magnitude, indicating that P_{NBI}^{i} is in balance with q_i. The electron heating power P_{NBI}^{e} also has a variation similar to q_e, but the magnitude of q_e is slightly smaller compared to P_{NBI}^{e} in CW discharges. This can be attributed to other power sink terms such as radiation P_{rad} and convective power loss terms P_{conv}. Figure 8 shows that the contribution of P_{rad} and P_{conv} are higher for CW discharges in most pairs, and therefore relatively less power is transported by q_e in CW discharges as compared to the ILW counterparts.

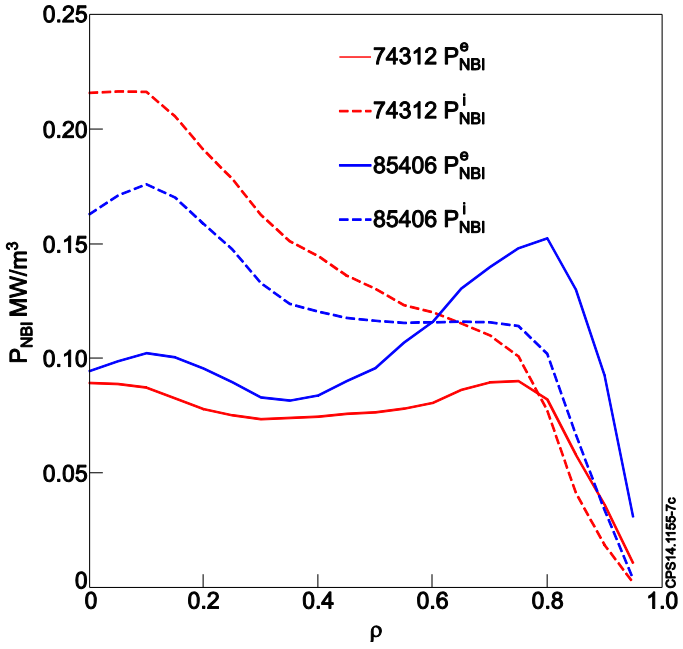

Figure 9 NBI power deposition to electron (solid) and ion (dotted) in JET-ILW (blue) and the counterpart JET-CW(red).

The difference in NBI power deposition between CW discharges and the ILW counterparts can be clearly seen in Figure 9, for one pair of discharges from the database. The total deposited P_{NBI} ($= P_{NBI}^{e} + P_{NBI}^{i}$) in the ILW discharge is shifted towards the edge (ρ ~0.8). Since the same total NBI power is applied to the both discharges, this implies that in ILW discharges slightly less NBI power is deposited into the core. This can be seen in Figure

10(a) showing that the total deposited P_{NBI} within the volume ρ<0.5 in ILW discharges is smaller than that in the CW counterparts.

Within the total deposited NBI power P_{NBI} ($=P^{e}_{NBI}+P^{i}_{NBI}$), the fraction of electron and ion heating is a function of local ε_b/T_e, with higher ε_b/T_e resulting in lower ion and higher electron heating fractions [18]. The average value of ε_b/T_e within the volume ρ <0.5 is shown in Figure 10(b). ILW discharges have higher ε_b/T_e than their counterpart CW discharges due to the lower core T_e. Therefore the fraction of total NBI power deposition to electrons is larger for ILW plasmas as compared to the CW counterparts. Hence, as can be seen in Figure 7(f) and 9, the heating efficiency of electrons (P^{e}_{NBI}) within the volume ρ <0.5 is larger in ILW plasmas despite the reduction of total NBI power deposition. On the other hand, both the fraction of core ion heating and the total NBI deposition are higher for CW plasmas, which results in much greater core P^{i}_{NBI}. In summary, the analysis above shows that for the same total NBI power, core electron heating is more efficient in ILW plasmas while ion heating is reduced. It should be noted that the lower fraction of core ion heating in ILW plasmas is attributed to the lower edge T_e, which suggests that by recovering the edge electron temperature, the differences in profile of NBI power deposition between ILW and CW plasmas might be removed.

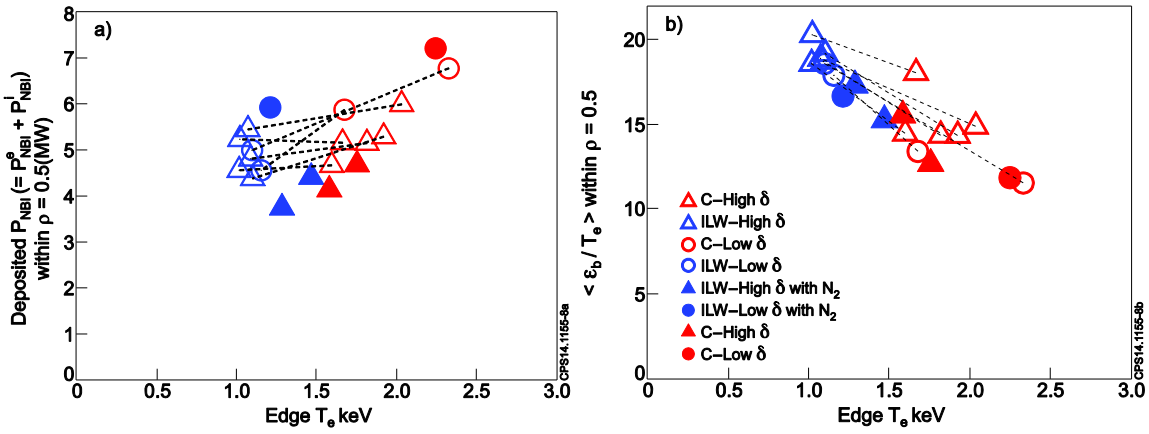

Figure 10 (a) Total deposited beam power P_{NBI} ($=P^{e}_{NBI}+P^{i}_{NBI}$) within the volume ρ < 0.5 (b) averaged value of ε_b/T_e over the volume ρ < 0.5. Each dashed line indicates the counterpart data to show the change of the data from the CW to the ILW. The notation of colour and symbols are same as described in Figure 5.

During the steady state, the electrons (τ^{e}_{core}), ions (τ^{i}_{core}), and plasma (τ^{e+i}_{core}) energy confinement time in the volume within ρ <0.5 are calculated as

$$\tau^{e}_{core}(\rho<0.5)=\frac{\int_0^{V'(\rho=0.5)} W^{e}_{th}(\rho)\,dV}{\int_0^{V'(\rho=0.5)} P^{e}_{Total}(\rho)\,dV}$$

$$\text{where } W^{e}_{th}(\rho)=\frac{3}{2}(n_e(\rho)T_e(\rho)-n_e(\rho=0.5)T_e(\rho=0.5)),$$

$$\tau^{i}_{core}(\rho<0.5)=\frac{\int_0^{V'(\rho=0.5)} W^{i}_{th}(\rho)\,dV}{\int_0^{V'(\rho=0.5)} P^{i}_{Total}(\rho)\,dV} \qquad (2)$$

$$\text{where } W^{i}_{th}(\rho)=\frac{3}{2}(n_i(\rho)T_i(\rho)-n_i(\rho=0.5)T_i(\rho=0.5)),$$

$$\tau^{e+i}_{core}(\rho<0.5)=\frac{\int_0^{V'(\rho=0.5)} W^{e+i}_{th}(\rho)dV}{\int_0^{V'(\rho=0.5)} P^{e+i}_{total}(\rho)\,dV}$$

$$\text{where } W^{e+i}_{th}(\rho)=W^{e}_{th}(\rho)+W^{i}_{th}(\rho), \text{ and } P^{e+i}_{total}(\rho)=P^{e}_{total}(\rho)+P^{i}_{total}(\rho).$$

W^{e}_{th} and W^{i}_{th} are the stored core thermal energy in electrons and ions, and P^{e}_{total} and P^{i}_{total} are the total heating power to electrons and ions, respectively. Figure 11 shows that W^{e}_{th} and W^{i}_{th} in ILW plasmas are clearly decreased compared to the CW counterparts, as observed by the lower core T_e in ILW. However, τ^{i}_{core} in ILW plasmas is not reduced compared to the CW counterparts since P^{i}_{total} is also lower in ILW plasmas. In other words, this implies that the smaller W^{i}_{th} in ILW plasmas is just due to the smaller ion heating in the core, rather than degradation of the core ion confinement. P^{e}_{total} is slightly higher in ILW plasmas, and this leads to smaller τ^{e}_{core}. As a result, the plasma energy confinement time τ^{e+i}_{core} is slightly smaller in ILW plasmas.

As observed in Figure 5, by recovering edge temperature the core temperature in JET-ILW approaches the values in the CW counterparts, and this would lead to comparable core energy in JET-ILW. The difference in the core beam heating fraction would be also removed by recovering edge T_e, as it is determined by the core T_e. Therefore, it is expected

that the core energy confinement time with a fully recovered edge T_e in JET-ILW will be similar with JET-CW.

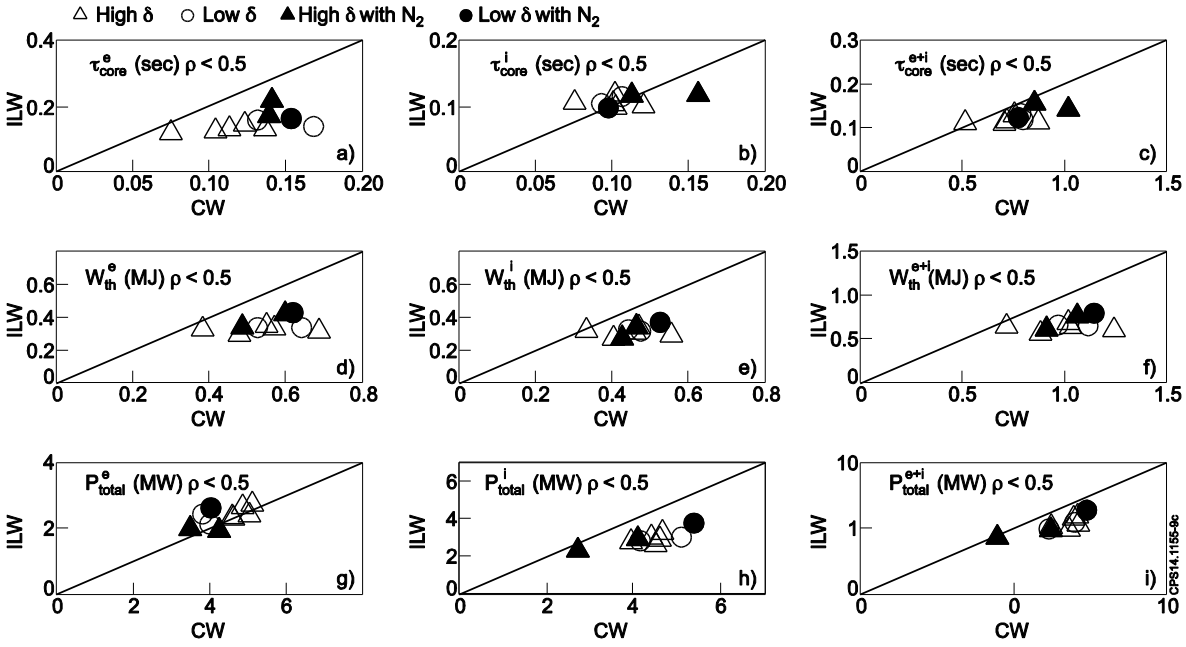

Figure 11 Comparison of energy confinement time in the volume within ρ <0.5: (a)electrons τ^e_{core}, (b) ions τ^i_{core}, (c)plasma τ^{e+i}_{core} between ILW and the counterpart in CW. Comparison of the stored thermal energy in the volume within ρ <0.5: (d)electrons W^e_{th}, (e) ions W^i_{th}, (f)plasma W^{e+i}_{th}. Comparison of the total heating power in the volume within ρ <0.5: (g)electrons P^e_{total}, (h) ions P^i_{total}, (i)plasma P^{e+i}_{total}.

4 DISCUSSION

Although equal electron and ion temperature profiles is assumed for all TRANSP simulations in this analysis, there is a possibility that the core ion temperature is higher than the electron temperature in CW discharges due to higher NBI ion heating as compared to ILW discharges. The green filled triangles in Figure 7 indicate the TRANSP results for a CW discharge assuming slightly higher T_i profile i.e. T_i=1.05xT_e. Due to the high equilibration power, heat fluxes and conductivities can be changed by even a small discrepancy in T_i and T_e, while the NBI heat deposition is not sensitive to the change in T_i. Thus, with a slightly higher T_i, the CW plasma has higher q_i and χ_i and lower q_e and χ_e, making it more similar to its ILW counterpart. This implies that the value of the calculated heat transport coefficients

can be affected by a large uncertainty. However, the above uncertainty does not affect the energy confinement calculation as the sum of heat-flux-power-loss and equilibration-power-loss does not depend on the assumption on T_i (i.e. same total power loss). Hence, the conclusion made by comparing the core energy confinement time remains valid despite the uncertainty in the T_i profiles.

The lack of agreement between the measured and the calculated beam-target neutron rates is an issue in many tokamaks including JET. It was reported that in order to reproduce JET neutron rate measurements for high density baseline JET plasmas, which is the same case analysed in the paper, an anomalous radial transport diffusivity of the fast ions of the order of 5-10 m^2s^{-1} needs to be included in TRANSP simulations [19] [20]. This issue was also observed in other devices such as ASDEX Upgrade [21], DIII-D [22] [23], and MAST [24]. Figure 12 compares the neutron rate measured by Fission chamber [25] which was calibrated in 2013 [26], and the neutron rate calculated by TRANSP (without anomalous fast ion diffusivity). As dominant neutrons are generated by the fusion reaction between beam fast ions and thermal ions, without a model for fast ion anomalous transport in TRANSP, the calculated neutron rates are always higher than the measured value i.e. there is a neutron deficit in the measurement. However, the fraction of neutron deficit is around 30% for all the discharges, as can be seen by the linear alignment in Figure 12. This indicates that the neutron deficit with respect to the fast ion model in TRANSP is the same for all the discharges, and therefore does not have an impact on the comparative analysis between CW and ILW plasmas. In addition, the consistent neutron deficit fraction implies that uncertainty in neutral density or Z_{eff}, which can affect neutron production through fast ion losses or ion dilution, respectively, should be small in the database.

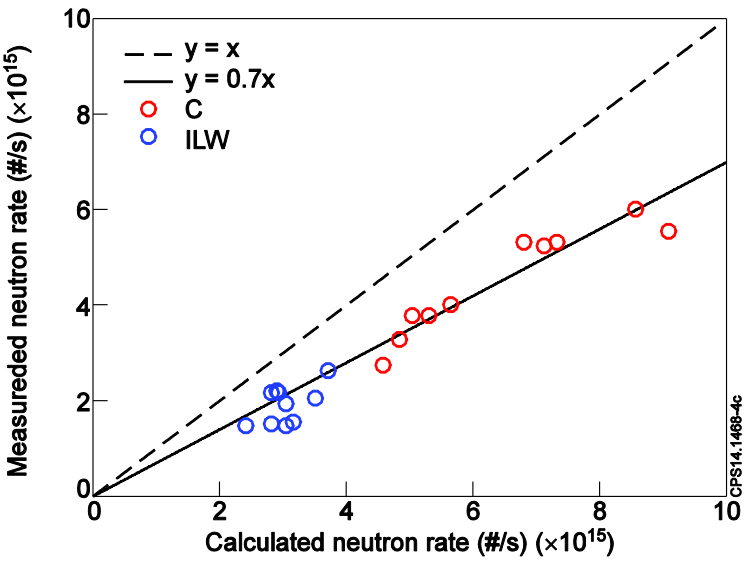

Figure 12 Comparison between the measured neutron rate and the TRANSP calculated neutron rate

5 CONCLUSION

In this paper we have investigated the core transport of high density JET H-mode discharges to assess whether core confinement has been affected by the change of PFCs. To address the above question, a comparative analysis of the core transport of similar H-mode plasmas with Carbon and ITER-like wall has been presented. The discharges analysed have been carefully selected to have the same main global parameters so that any difference in core transport and confinement can be ascribed to effects linked to the different wall composition or different scenario operation.

Similar temperature peaking is observed in both ILW and C-wall plasmas. When ILW discharges are seeded with N_2, both core and edge T_e increase to maintain a similar peaking factor. The analysis carried out with interpretative TRANSP simulations shows that in ILW discharges higher NBI power is deposited towards the plasma edge ($\rho>0.6$), reducing by 1~2 MW the power deposited in the central region ($\rho<0.5$). Lower electron temperature is consistently observed at the top of the pedestal of ILW discharges; as a result, the fraction of NBI power deposited to the ions is reduced while the fraction of NBI power to the electrons is increased. This implies that the core electron energy confinement time is somewhat smaller in ILW discharges, but the core ion energy confinement time is not changed.

The analysis reported in this paper indicates that the overall core energy confinement is not degraded in the ILW discharges as compared to the CW counterparts. Since the NBI power deposition and core ion transport depend strongly on the electron temperature profile, it is likely that high core electron temperatures (comparable to that in CW) and improved plasma performance would be achieved if the edge T_e were recovered.

Acknowledgments

This work has been carried out within the framework of the EUROfusion Consortium and has received funding from the Euratom research and training programme 2014-2018 under grant agreement number 633053, and from the RCUK Energy Programme [grant number EP/I501045]. The views and opinions expressed herein do not necessarily reflect those of the European Commission. The authors appreciate the scientific coordinators of the CW discharges at JET, S. Brezinsek, T. Loarer, D. McDonald, P. Lang, and G. Saibene.

6 BIBLIOGRAPHY

[1] M. Beurskens, et al, "The effect of a metal wall on confinement in JET and ASDEX Upgrade," *Plasma Physics and Controlled Fusion,* vol. 55, no. 12, p. 124043, 2013.

[2] G. Matthews, et al, "JET ITER-like wall overview and experimental programme," *Physica Scripta,* vol. 2011, no. T145, p. 014001, 2011.

[3] J. Schweinzer, et al, "Confinement of improved H-modes in the all-tungsten ASDEX Upgrade with nitrogen seeding," *Nuclear Fusion,* vol. 51, no. 11, p. 113003, 2011.

[4] M. Beurskens, et al, "Global and pedestal confinement in JET with a Be/W metallic wall," *Nuclear Fusion,* vol. 54, no. 4, p. 043001, 2014.

[5] J. Hobirk, et al, "Improved confinement in JET hybrid discharges," *Plasma Physics and Controlled Fusion,* vol. 54, no. 9, p. 095001, 2012.

[6] C. D. Challis, et al, "Improved Confinement in JET High Beta Plasmas with an ITER-Like Wall," *Nuclear Fusion,* 2014 (submitted).

[7] R.Goldston, et al, "New techniques for calculating heat and particle source rates due to neutral beam injection in axisymmetric tokamaks," *Journal of Computational Physics,* vol. 43, no. 1, pp. 61-78, 1981.

[8] R. Hawryluk, "An empirical approach to tokamak transport," in *Physics of Plasmas close to Thermonuclear Conditions*, 1979.

[9] R. Pasqualotto, et al, "High resolution Thomson scattering for Joint European Torus (JET)," *Review of Scientific Instruments,* vol. 75, p. 3891, 2004.

[10] L. Ingesson, "The Mathematics of some Tomography Algorithms at JET," JET Reports JET-R(99)08, 1999.

[11] L. Lao, et al, "Reconstruction of current profile parameters and plasma shapes in

tokamaks," *Nuclear Fusion,* vol. 25, no. 11, p. 1611, 1985.

[12] C. Giroud, et al, "Impact of nitrogen seeding on confinement and power load control of a high-triangularity JET ELMy H-mode plasma with a metal wall," *Nuclear Fusion,* vol. 53, no. 11, p. 113025, 2013.

[13] H. Meister, et al, "Zeff from spectroscopic bremsstrahlung measurements at ASDEX Upgrade and JET," *Review of Scientific Instruments,* vol. 75, no. 10, pp. 4097-4099, Oct 2004.

[14] K. Mast, et al, "Bolometric diagnostics in JET," *Review of Scientific Instruments,* vol. 56, no. 5, pp. 969-971, May 1985.

[15] R. Budny, et al, "Progress Testing TRANSP-TORIC Simulations of ICRH in JET," in *36th EPS conference on plasma physics*, Sofia, Bulgaria, 2009.

[16] J. Ongena, et al, "Numerical Transport Codes," *Transactions of Fusion Science and Technology,* vol. 33, pp. 181-191, 1998.

[17] S. I. Braginskii, "Transport Processes in a Plasma," *Reviews of Plasma Physics,* vol. 1, p. 205, 1965.

[18] J. Wesson, et al, Tokamaks, CLARENDON PRESS OXFORD, 2004.

[19] Yu. Baranov, et al, "Anomalous and classical neutral beam fast ion diffusion on JET," *Plasma Physics and Controlled Fusion,* vol. 51, no. 4, p. 044004, 2009.

[20] M. Nocente et al, "Neutron spectroscopy measurements of tritium beam transport at JET," *Nuclear Fusion,* vol. 54, no. 10, p. 104010, 2014.

[21] e. a. S. Gunter, "Interaction of energetic particles with large and small scale instabilities," *Nuclear Fusion,* vol. 47, no. 8, p. 920, 2007.

[22] M. Murakami, et al, "Progress toward fully noninductive high beta conditions in DIII-D," *Physics of Plasmas,* vol. 13, no. 5, pp. -, 2006.

[23] E.M. Carolipio et al, "Simulations of beam ion transport during tearing modes in the DIII-D tokamak," *Nuclear Fusion,* vol. 42, no. 7, p. 853, 2002.

[24] D.L. Keeling et al, "Mitigation of MHD induced fast-ion redistribution in MAST and implications for MAST-Upgrade design," *Nuclear Fusion,* vol. 55, no. 1, p. 013021, 2015.

[25] M. T. Swinhoe, et al, "Calculation and measurement of 235U and 238U fussion counter assembly detection efficiency," *Nuclear Instruments and Methods in Physics Research,* vol. 221, no. 2, pp. 460-465, 1984.

[26] D.B. Syme, et al, "Fusion yield measurements on JET and their calibration," *Fusion Engineering and Design,* vol. 89, no. 11, pp. 2766-2775, 2014.